



HAL
open science

Tropospheric ozone retrieval from thermal infrared nadir satellite measurements: Towards more adaptability of the constraint using a self-adapting regularization

Maxim Eremenko, Luca Sgheri, Marco Ridolfi, Juan Cuesta, Lorenzo Costantino, Pasquale Sellitto, Gaelle Dufour

► To cite this version:

Maxim Eremenko, Luca Sgheri, Marco Ridolfi, Juan Cuesta, Lorenzo Costantino, et al.. Tropospheric ozone retrieval from thermal infrared nadir satellite measurements: Towards more adaptability of the constraint using a self-adapting regularization. *Journal of Quantitative Spectroscopy and Radiative Transfer*, 2019, 238, pp.106577. 10.1016/j.jqsrt.2019.106577 . hal-02365313

HAL Id: hal-02365313

<https://hal.science/hal-02365313>

Submitted on 21 Dec 2021

HAL is a multi-disciplinary open access archive for the deposit and dissemination of scientific research documents, whether they are published or not. The documents may come from teaching and research institutions in France or abroad, or from public or private research centers.

L'archive ouverte pluridisciplinaire **HAL**, est destinée au dépôt et à la diffusion de documents scientifiques de niveau recherche, publiés ou non, émanant des établissements d'enseignement et de recherche français ou étrangers, des laboratoires publics ou privés.



Distributed under a Creative Commons Attribution - NonCommercial 4.0 International License

Tropospheric ozone retrieval from thermal infrared nadir satellite measurements: towards more adaptability of the constraint using a self-adapting regularization.

Eremenko Maxim^{a,*}, Sgheri Luca^b, Ridolfi Marco^{c,d}, Cuesta Juan^a, Costantino Lorenzo^a, Sellitto Pasquale^a, Dufour Gaëlle^a

^a*Laboratoire Inter-universitaire des Systèmes Atmosphériques (LISA), UMR7583, CNRS, Université Paris-Est Créteil, Université de Paris, Institut Pierre Simon Laplace, Créteil, France*

^b*Istituto per le Applicazioni del Calcolo, Consiglio Nazionale delle Ricerche, Firenze, Italy*

^c*Dipartimento di Fisica e Astronomia, Università di Bologna, Italy*

^d*Istituto Nazionale di Ottica, Consiglio Nazionale delle Ricerche, Firenze, Italy*

Abstract

We developed a Self-Adapting Constraint Retrieval Scheme (SACRS) to retrieve ozone profiles from nadir infrared satellite measurements. In this algorithm, the constraint is variable in altitude and adapted automatically for each individual measurement. The algorithm is tested on synthetic observations representing the future IASI-NG satellite observations and considering either ozonesonde measurements or chemistry-transport model ozone simulations to represent the true ozone (pseudo-reality). The ozone retrievals are evaluated mainly for the troposphere with a specific focus on the lower troposphere between the surface and 6 km. Compared to a previous algorithm based on a fixed constraint retrieval scheme (FCRS), the biases, correlation and error estimates are improved with the SACRS. The bias is reduced by 40% and the correlation coefficient increases from 0.72 to 0.80. The SACRS algorithm also leads to an enhanced sensitivity in the lower troposphere with degrees of freedom for signal up to 0.83, increased by 11% compared to the FCRS. The SACRS performs especially well where current algorithms usually fail, namely for polar and tropical air masses.

*Corresponding author
E-mail address: maxim.eremenko@lisa.u-pec.fr

The bias is reduced from 8.6% to 0.5% in the troposphere (surface-9 km) when considering polar cases and from 24.4% to 10.1% in the upper troposphere lower tropospheric column (12-18 km) in the tropics.

Keywords: Atmospheric composition, Air pollution monitoring, Ozone, Passive remote sensing, Inverse problems.

1. Introduction

Tropospheric ozone is a key species for tropospheric chemistry, air quality and radiative balance. Its monitoring is essential to better understand sources, transport, chemical transformation and sinks of atmospheric pollutants. Accurate data are required to characterize the evolution of atmospheric composition. 5 Space-borne observations are very promising for these concerns. Several studies using the last generation satellite instruments, in particular those operating in the thermal infrared, like the Infrared Atmospheric Sounding Interferometer (IASI) [1], have shown capabilities to detect and monitor pollution events 10 [2, 3, 4] and to identify the influence of the meteorology, horizontal transport and exchange with the stratosphere on tropospheric ozone variability and trends [4, 5, 6, 7, 8, 9]. Even so, lower tropospheric ozone retrievals from nadir sounders remain challenging due to the lack of sensitivity of the measurements to the composition of near-surface layers. Even if improvements have been made especially 15 combining the information provided by multiple spectral regions and instruments, as done by synergism of infrared and ultraviolet observations [10, 11], it is still important to explore possibilities to improve the adaptability of the retrieval algorithms and their capability to exploit the information provided by any kind of satellite measurements. The ozone retrieval from nadir satellite 20 observations, in fact, is an ill-conditioned problem which requires regularization using constraints and a priori information [12]. Up to now, most of the retrieval algorithms rely on a fixed constraint and a single a priori profile. The most widely used method is the optimal estimation approach [13, 14] based on a priori ozone climatological constraint. There are some other attempts to develop

25 infrared nadir retrievals such as the physical retrieval methods [15, 16], where the
a priori covariance constraint has an additional regularization parameter: scalar
coefficient that may be adjusted to tune the trade off between data and a pri-
ori constraint. Another class of retrieval methods uses an analytical constraint
based on Tikhonov-Twomey type regularization ([17, 18, 19]) in place of the a
30 priori covariance [20, 2]. The regularization strength in these retrieval meth-
ods is adjusted by the minimisation scheme based on the Levenberg-Marquardt
method [21, 22]. A number of validation studies including some of these retrieval
schemes shows that all these approaches provide globally comparable, though
not identical, results in terms of the accuracy of the retrieval [23, 24]. In the fol-
35 lowing, one of these algorithms used by the authors in previous studies for IASI
retrievals [2] will be referred to as Fixed Constraint Retrieval Schemes (FCRS).
This approach, as well as the optimal estimation technique, works satisfacto-
rily for most retrieval scenes, but in some situations both methods may lead
to difficulties in reproducing the natural variability of ozone and in correctly
40 describing its vertical distribution. Independent validation studies of different
retrieval methods mention these difficulties for the IASI [24, 25] and the TES
[26, 27] ozone profile retrievals. Larger biases are found, e.g. in higher latitudes
that are usually attributed to the reduced sensitivity of the infrared measure-
ments in these regions due to unfavourable thermal conditions (low thermal
45 contrast and cold tropospheric temperatures). Larger biases are also showed in
the upper troposphere - lower stratosphere (UTLS), for some tropical scenes,
that may possibly be explained by the limited vertical resolution of the retrieval
in the infrared, spectroscopic uncertainties, or the use of inadequate a priori
information [24, 25]. These profiles retrieval difficulties are illustrated for the
50 case of TES instrument in figure 2 of [26] and figure 4 of [27], and for the IASI
instrument in figure 14 of [25] and figure 13 of [24]. Figure 10 of the present
study shows similar retrieval problems for the case of FCRS. One of the moti-
vations for the SACRS development was the necessity to tackle these retrieval
limitations. In the present study, we propose to go a step further by developing
55 a Self-Adapting Constraint Retrieval Scheme (SACRS) in which the constraint,

dependent on altitude, is derived for each individual measurement while using a large choice of multiple a priori profiles. The objective is to better exploit the information provided by satellite measurements, adapting the retrieval to the atmospheric scenario, and to finally derive more accurate ozone vertical profiles.

60 We evaluate the potential of this new approach for the future satellite instrument IASI-NG (IASI Next Generation), which is expected to provide more spectral information on the ozone vertical profile than IASI [31, 32]. This instrument is expected to be launched in 2022 as part of the EPS-SG (EUMETSAT Polar System-Second Generation) mission. Its spectral and radiometric performances
65 are twice better than those of the IASI instruments [31], with an apodized spectral resolution of 0.25 cm^{-1} and radiometric noise of $10 \text{ nW}/(\text{cm}^2\text{srcm}^{-1})$ in the $10 \mu\text{m}$ ozone band. Studies using FCRS retrieval algorithms like those used for IASI show that the improved instrumental performances of IASI-NG will lead to an improved vertical resolution both over land and over sea [31, 32].
70 The SACRS algorithm has been tested on synthetic observations matching the future IASI-NG satellite instrumental characteristics and compared to results obtained with the FCRS algorithm previously developed for IASI [2] and applied to IASI-NG. For both retrieval schemes, as for the IASI retrievals, the seven spectral windows have been used for O_3 retrieval. In the case of these
75 spectral regions and IASI-NG spectral resolution, the measurement vector is composed of 559 spectral radiances. Within this simulation exercise the surface temperatures and the atmospheric temperature profiles are considered as known. The developed multiple a priori and SACRS approach are described in section 2. The pseudo-observation setup and the correlative database as well
80 as the simulation experiments are summarized in section 3. Section 4 discusses the results of the simulation experiments performed from the model simulations and the ozonesondes measurements. Conclusions are given in section 5.

2. SACRS approach

The new SACRS approach is the combination of two previously developed
85 algorithms: a retrieval method of lower tropospheric ozone from the IASI nadir
sounder, originally implemented as a FCRS and used for different studies:
[2, 3, 4, 5, 6, 7], and the Iterative Variable Strength (IVS) technique [33, 34],
initially conceived as a self-adapting approach for the Michelson Interferometer
for Passive Atmospheric Sounding (MIPAS) limb sensor and now the operative
90 choice for the MIPAS retrievals made by the European Space Agency (ESA) [35].
The SACRS algorithm consists of two steps, both containing a self-adapting fea-
ture. The first step enhances the choice of a priori profiles made for the FCRS
algorithm, by modifying the fixed a priori error profiles in order to obtain a less
constrained retrieval. The retrieval is then carried out with this weak constraint,
95 in order to maximize the number of degrees of freedom of the solution. This
also decreases the bias introduced by the a priori. The result is an oscillating
profile with large error bars. In the second and final step, the IVS method adds
an a posteriori regularization with an altitude dependent strength determined
primarily by the measurement errors and the sensitivity of the actual measure-
100 ments to the retrieved profile. The result is a smooth profile with a reduced
bias with respect to the original FCRS method.

2.1. Enhanced choice of multiple a priori profiles

The choice of a priori profiles in the FCRS used in this study is based on
averaged ozone profiles derived from climatology for three geographical zones
105 (polar, midlatitudes and tropics) [2]. The terms 'polar', 'midlatitudes' and
'tropics' define here the type of the air masses according to the tropopause height
and not the geographical coordinates. For example, the polar-type air masses are
characterised by a low tropopause height (TPH) even when transported off the
polar region. The chosen discriminant parameter is TPH with polar conditions
110 defined as observed scenes with TPH lower than 10 km, midlatitudes conditions:
TPH between 10 km and 14 km, and tropical conditions: TPH greater than 14
km.

This is a first approach for adapting the retrieval for the measuring conditions which shows reliable validation results [24, 4]. However, some ozone profile shapes, especially in the upper troposphere, remain penalized and lead to spurious oscillations in the retrieved profiles, especially for tropical-like atmosphere [24, 25]. As the vertical resolution (the altitude range of the independent pieces of information) of nadir sounders like IASI or IASI-NG is limited (5-7 km), retrieving the strong vertical ozone variability in the upper troposphere – lower stratosphere is challenging. Introducing reliable a priori information may help to partly overcome the problem. As the first step of the SACRS approach, we developed a new set of a priori ozone profiles. We moved from a set of three a priori profiles to a set of eleven a priori profiles covering the TPH range between 7 km to 17 km. The new set of a priori profiles has been built using the ozone soundings provided by the networks of sounding stations such as World Ozone and Ultraviolet Radiation Data Centre (WOUDC), Southern Hemisphere Additional Ozonesondes (SHADOZ) and Global Monitoring Division (GMD). Over 10,000 ozone soundings measured between 2004 and 2007 were used to calculate the average ozone profiles grouped on the basis of TPH. Fig. 1 shows these ozone profiles and the three climatological a priori used for the FCRS. The comparison of these two sets of a priori profiles and their influence on the quality of the retrieval was made using both sets for the FCRS retrievals (see section 4). The TPH-dependent a priori profiles are used as the first guess in all simulated retrievals presented in this paper.

2.2. Retrieval bases and the FCRS

The details of the FCRS method used in this study in order to compare with the new SACRS approach are described in [2]. For FCRS, the optimal solution \mathbf{x}_F is defined as

$$\mathbf{x}_F = \mathbf{x}_k + (\mathbf{K}_k^T \mathbf{S}_y^{-1} \mathbf{K}_k + \mathbf{R})^{-1} [\mathbf{K}_k^T \mathbf{S}_y^{-1} (\mathbf{y} - \mathbf{F}(\mathbf{x}_k)) + \mathbf{R}(\mathbf{x}_a - \mathbf{x}_k)], \quad (1)$$

where k is the iteration counter, \mathbf{y} is the m -dimensional vector of the spectral observations with radiometric noise covariance matrix \mathbf{S}_y . The function \mathbf{F} is the

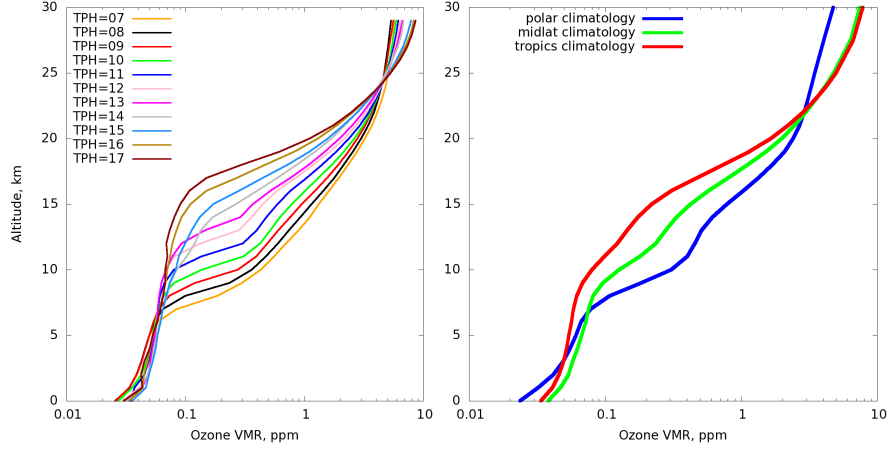


Figure 1: A priori ozone profiles as the function of TPH (left panel) used in SACRS, a priori ozone profiles as the function of the climatological zone (right panel) used in [2].

radiative transfer model, depending on the n -dimensional atmospheric state vector \mathbf{x} given in Volume Mixing Ratio (VMR), where $(\mathbf{x})_i = x(z_i)$ for a chosen altitude grid z_i . The matrix \mathbf{K}_k is the Jacobian of \mathbf{F} evaluated at iteration k . In the FCRS approach \mathbf{R} is a fixed altitude-dependent matrix constraining the solution towards the a priori estimate \mathbf{x}_a , and defined to fulfil a chosen criterion. Different methods to determine the criterion are described in [36]. The criterion used for FCRS in this study is based on a compromise between the minimization of the retrieved profile error and the maximization of the degrees of freedom (DOF) of the solution in the lower troposphere. In addition to the strength and shape of the constraint (diagonal elements of the \mathbf{R} matrix) used to regularize the values and the general shape of the retrieved profile, the first or the second derivative operators (off-diagonal elements of the \mathbf{R} matrix) are necessary to establish the inter-layer correlations and thus to limit the oscillations of the retrieved vertical profile [2].

The Averaging Kernel (AvK) of the FCRS solution is given by:

$$\mathbf{A}_F = (\mathbf{K}_k^T \mathbf{S}_y^{-1} \mathbf{K}_k + \mathbf{R})^{-1} (\mathbf{K}_k^T \mathbf{S}_y^{-1} \mathbf{K}_k), \quad (2)$$

and the a posteriori covariance matrix of the parameters due to the mapping of

the measurement noise into the solution is:

$$\mathbf{S}_{F,m} = (\mathbf{K}_k^T \mathbf{S}_y^{-1} \mathbf{K}_k + \mathbf{R})^{-1} (\mathbf{K}_k^T \mathbf{S}_y^{-1} \mathbf{K}_k) (\mathbf{K}_k^T \mathbf{S}_y^{-1} \mathbf{K}_k + \mathbf{R})^{-1}. \quad (3)$$

If \mathbf{S}_a is a covariance matrix representing the atmospheric variability of the profile \mathbf{x} , the covariance matrix of the smoothing error [12] of the solution is given by:

160

$$\mathbf{S}_{F,s} = (\mathbf{I} - \mathbf{A}_F) \mathbf{S}_a (\mathbf{I} - \mathbf{A}_F)^T, \quad (4)$$

where \mathbf{I} is the identity matrix.

The covariance matrix of the total error for the FCRS solution is:

$$\mathbf{S}_{F,tot} = \mathbf{S}_{F,m} + \mathbf{S}_{F,s}. \quad (5)$$

2.3. SACRS

As mentioned above, in FCRS approaches, the strength and the off-diagonal
 165 components of the regularization matrix \mathbf{R} are similar for all the measurements. This can lead to under- or over-constraining the solution, depending if the thermal conditions of the measurement are favorable or not to the retrieval. As a consequence, the retrieval may have difficulties to reproduce correctly the natural ozone variability. To overcome this problem and ensure an efficient use
 170 of the satellite instrument capabilities, we propose the new SACRS approach which is a two-step retrieval scheme.

The rationale behind the SACRS approach is to couple the FCRS regularization with variable constraint and a priori, with the IVS a posteriori self-adapting regularization method. The IVS is not meant to be used during the iterations
 175 because the target function to minimize would be modified by the change of the regularization matrix \mathbf{R} . This would introduce instabilities in the retrieval iterations, and slow down the convergence, as explained in [33]. Thus, the IVS should be used as an a posteriori regularization. However, in order to make the application of the IVS method possible and effective, we need a converg-
 180 ing retrieval, with the weakest possible constraint $\tilde{\mathbf{R}}$. This will minimize the bias introduced by the smoothing, whilst the IVS will take care of dumping the

oscillations in the altitude regions where the sensitivity of the measurement is weak.

2.3.1. Weak constraint solution

185 The definition of the weak constraint is based on the diagonal elements of the \mathbf{R} matrix developed for the IASI retrievals [2]. This diagonal is shifted, scaled and/or stretched to build the diagonal of the weak constraint matrix $\tilde{\mathbf{R}}$.

Let $f(z)$ be a generic function of the altitude z to be scaled, shifted or stretched.

190 The scaled function is written:

$$f_{\text{scale}}(z) = af(z) \quad (6)$$

with a the strength coefficient of the scaling.

The shifted function is written with its shift coefficient b

$$b > 0 \begin{cases} f_{\text{shift}}(z) = f(z + b), & z \in [0, n - b] \\ f_{\text{shift}}(z) = f(n), & z \in]n - b, n] \end{cases}$$

$$b < 0 \begin{cases} f_{\text{shift}}(z) = f(z + b), & z \in [-b, n] \\ f_{\text{shift}}(z) = f(0), & z \in [0, -b[\end{cases}$$

195 The stretched function is written:

$$f_{\text{stretch}}(z) = f^c(z) \quad (7)$$

where c is the stretching coefficient.

These resulting transformations are illustrated by the Fig. 2.

The function combining scaling, shifting and stretching is written:

$$\tilde{f}(z) = af_{\text{shift}}^c(z) \quad (8)$$

200 Applying this function to the retrieval altitude grid $z \subset [0, n]$, the constraint vector \tilde{f}_v is obtained.

The weak constraint matrix is then:

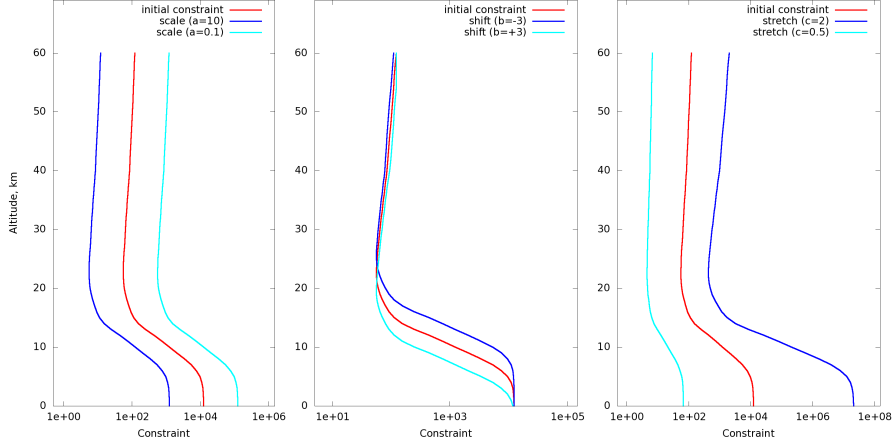


Figure 2: Scaling, shifting and stretching applied to the constraint function in order to find the weak constraint adapted to a particular measurement.

$$\tilde{\mathbf{R}} = \begin{bmatrix} \tilde{f}_v(0) & 0 & 0 & \dots & 0 \\ 0 & \tilde{f}_v(1) & 0 & \dots & 0 \\ \vdots & & \ddots & & \\ 0 & 0 & 0 & \dots & \tilde{f}_v(n) \end{bmatrix}$$

The a, b, c coefficients in Eq. 8, are allowed to vary within the predefined ranges: $a \in [10^{-2}, 10^5]$, $b \in [-5, 5]$, $c \in [0.3, 3]$. The a, b, c coefficients are chosen to minimize the target function φ :

$$\varphi = c_1 * \frac{1}{N_{ex}} + c_2 * RMS + c_3 * \frac{1}{\sqrt{DOF_6}} + c_4 * H_6^{max} \quad (9)$$

205 where

– N_{ex} is the number of extremal (maximum or minimum) points of the retrieved profile under 20 km. This parameter is chosen in order to control the oscillation in the tropospheric/stratospheric part of the retrieved profile,

– RMS is the root mean square of the spectral fit . This parameter is used
210 to control the quality of the spectral fit,

– DOF_6 is the DOF between the surface and 6 km of altitude. This parameter allows maximizing the AvK values in the lower troposphere,

– H_6^{max} is the height of maximum of sensitivity to ozone between the surface and 6 km. The value of H_6^{max} is calculated as the altitude of the maximum of the function obtained by the sum of the first 6 rows of the AvK matrix. This allows
 215 to estimate to which altitudes the measured partial column is most sensitive [10]. The parameter is chosen to control the altitude range of the AvK sensitivity in the lower troposphere.

The oscillating solution that is obtained at this stage is meant to have as
 220 many DOFs as possible. By maximizing the number of oscillations N_{ex} and keeping acceptable the *RMS* of the fit, we ensure that these multiple oscillations are taking place around the real atmospheric profile. The limit of 6 km for the DOF_6 and H_6^{max} is chosen taking into account the expected vertical resolution of IASI-NG in the lower troposphere [32]. The 6 km limit is used to optimise the
 225 retrieval of this lower tropospheric quantity. A more flexible definition of the criterion φ is also feasible. A different definition of the targeted partial column would imply different values for the coefficients used to compute φ , however the structure used for the φ function would not change.

The values of coefficients $c_{1,2,3,4}$ are chosen so that the four terms of φ have
 230 similar magnitudes. These coefficients do not change during the minimization of the target function.

The weak regularization is obtained at the first iteration of the retrieval by testing the combinations of a, b and c in order to minimize φ . In order to avoid calling numerous times the forward model, the choice of the parameters (a, b, c)
 235 is done using a linear approximation for calculating the radiance spectrum. This linear approximation of the spectrum is then used to calculate the spectral RMS difference with respect to measurements (which then allows the choice of the best parameters a, b, c). The linear approximation of the spectrum \mathbf{y}^{linear} is calculated using a single call of the forward model as follows

$$\mathbf{y}^{linear} = \mathbf{y}_a + \mathbf{K}_a(\mathbf{x}(a, b, c) - \mathbf{x}_a) \quad (10)$$

240 where:

– \mathbf{x}_a is the a priori state vector,
 – \mathbf{y}_a is the spectrum calculated with the forward model (KOPRA) for the a priori state vector \mathbf{x}_a ,

– \mathbf{K}_a is the Jacobian matrix calculated for \mathbf{x}_a ,
 245 – $\mathbf{x}(a, b, c)$ is the state vector obtained from inverse calculation (KOPRAFIT) using the R matrix which depends on the combination of the parameters (a, b, c) .

The ozone profile is then retrieved using the chosen weak regularization constraint. Subsequently the IVS approach is applied.

2.3.2. The IVS regularization technique

250 The IVS technique adapts the regularization strengths in the constraint matrix so as to regularize as strongly as possible, provided some pre-defined conditions are met by the regularized profile. The standard two conditions employed by the IVS technique are

- (i) At each altitude z_i the difference between the regularized and the oscillating profile should not exceed some fraction $w_e(z_i)$ of the retrieval error of the oscillating profile.
- 255 (ii) At each altitude z_i the vertical resolution of the regularized profile should not be degraded more than $w_r(z_i)$ times the vertical resolution of the unregularized profile.

260 We then start with a large regularization strength at all altitudes, and decrease it until conditions (i-ii) above are met, or the regularization strength is lower than a prescribed bound.

The SACRS solution \mathbf{x}_Λ is defined as

$$\mathbf{x}_\Lambda = \mathbf{x}_k + \left(\mathbf{K}_k^T \mathbf{S}_y^{-1} \mathbf{K}_k + \tilde{\mathbf{R}} + \mathbf{L}^T \Lambda \mathbf{L} \right)^{-1} \cdot \left[\mathbf{K}_k^T \mathbf{S}_y^{-1} (\mathbf{y} - \mathbf{F}(\mathbf{x}_k)) + (\tilde{\mathbf{R}} + \mathbf{L}^T \Lambda \mathbf{L})(\mathbf{x}_a - \mathbf{x}_k) \right], \quad (11)$$

where Λ is a diagonal semi-definite positive matrix, and \mathbf{L} is a matrix approximating some derivative of the vertical profile. We chose \mathbf{L} to be the $(n-1) \times n$
 265

matrix approximating the first derivative, so that

$$(\mathbf{L}\mathbf{x})_i \approx \frac{d}{dz} \mathbf{x}|_{(z_i+z_{i+1})/2}. \quad (12)$$

Hence we can interpret Λ as the sampling of a vertical profile $\lambda(z)$. Let $\tilde{z}_i = (z_i + z_{i+1})/2$, then $(\Lambda)_{ii} \equiv \lambda_i = \lambda(\tilde{z}_i)$. Following [34] we can connect \mathbf{x}_F and \mathbf{x}_Λ as

$$\mathbf{x}_\Lambda = \left(\mathbf{K}_k^T \mathbf{S}_y^{-1} \mathbf{K}_k + \tilde{\mathbf{R}} + \mathbf{L}^T \Lambda \mathbf{L} \right)^{-1} \cdot \left[\left(\mathbf{K}_k^T \mathbf{S}_y^{-1} \mathbf{K}_k + \tilde{\mathbf{R}} \right) \mathbf{x}_F + \mathbf{L}^T \Lambda \mathbf{L} \mathbf{x}_a \right]. \quad (13)$$

270 Also, the AvKs and the a posteriori covariance matrix of the IVS solution are connected to those of the FCRS solution by

$$\mathbf{A}_\Lambda = \mathbf{D} \mathbf{A}_F, \quad (14)$$

$$\mathbf{S}_{\Lambda, m} = \mathbf{D} \mathbf{S}_{F, m} \mathbf{D}^T, \quad (15)$$

where

$$\mathbf{D} = \left(\mathbf{K}_k^T \mathbf{S}_y^{-1} \mathbf{K}_k + \tilde{\mathbf{R}} + \mathbf{L}^T \Lambda \mathbf{L} \right)^{-1} \left(\mathbf{K}_k^T \mathbf{S}_y^{-1} \mathbf{K}_k + \tilde{\mathbf{R}} \right). \quad (16)$$

The smoothing error of the SACRS solution is given by:

$$\mathbf{S}_{\Lambda, s} = (\mathbf{I} - \mathbf{A}_\Lambda) \mathbf{S}_a (\mathbf{I} - \mathbf{A}_\Lambda)^T. \quad (17)$$

The covariance matrix of the total error is:

$$\mathbf{S}_{\Lambda, \text{tot}} = \mathbf{S}_{\Lambda, m} + \mathbf{S}_{\Lambda, s}. \quad (18)$$

275 Finally, to calculate the vertical resolution of the \mathbf{x}_Λ solution we use

$$\nu_i = \frac{\sum_{j=1}^n (\mathbf{A}_\Lambda)_{ij} (z_{j-1} - z_{j+1})}{2|\mathbf{A}_\Lambda|_{ii}}, \quad (19)$$

see [34] for the motivations.

We start with a constant profile $\lambda^{(0)}(z) = \lambda_{\max}$ and iterate the calculation of \mathbf{x}_Λ with decreasing profiles $\lambda^{(j+1)}(z) \leq \lambda^{(j)}(z)$.

Given the thresholds $w_e(z)$ and $w_r(z)$ we check the following two sets of
280 conditions

$$(i) |(\mathbf{x}_\Lambda)_i - (\mathbf{x}_F)_i| \leq w_e(z_i)\sqrt{(\mathbf{S}_F)_{ii}},$$

$$(ii) \nu_i \leq w_r(z_i)\Delta z_i,$$

and collect the altitudes $Q^{(j)} = \{z_{i_1}, \dots, z_{i_m}\}$ where these conditions are not met. In the MIPAS limb measurements [33, 34] the averaging kernels are mostly
 285 diagonal. Hence, to obtain a variation of the regularized profile at a given altitude it is sufficient to alter the regularization profile in a neighborhood of that altitude. Due to the different observation geometry this is not the case of the nadir measurements in which, for example, the most relevant information on ozone originates from the free troposphere and the lower stratosphere. Therefore
 290 we calculate the sensitivity coefficients $s_{ij} = \partial(\mathbf{x}_\Lambda)_i / \partial \lambda_j$, $i = 1, \dots, n$, $j = 1, \dots, n - 1$ in order to determine in which region the regularization profile has to be decreased to obtain a localized effect on the regularized profile. Let \tilde{l} such that $|s_{i\tilde{l}}| = \max_j \{|s_{lj}|\}$. Then for each altitude $z_l \in Q^{(j)}$ we decrease $\lambda(z)$ in a neighborhood of $z_{\tilde{l}}$. At each step j the new regularization profile $\lambda^{(j+1)}(z)$
 295 is the result of the combined application of the decreasing $\lambda(z)$ relative to the altitudes in $Q^{(j)}$. For details on how the reduction is performed we refer to [34]. We then repeat the calculation of \mathbf{x}_Λ and iterate the procedure until

$$(i) Q^{(j)} \text{ is empty, or}$$

$$(ii) \lambda(z) < \lambda_{\min}, \text{ or}$$

300 (iii) a maximal number of iterations is reached.

Note that the calculation of the sensitivity coefficients s_{ij} is equivalent to performing n iterations of the IVS, so they are updated only every 10 cycles. In the present implementation we use the following numerical values for the parameters driving the IVS algorithm: $w_e(z) = 1$, $w_r(z) = 1.5$, $\lambda_{\min} = 10^{-6}$,
 305 $\lambda_{\max} = 10$, maximal number of iterations equal to 1000. With these settings the typical running time of the IVS algorithm is a few seconds on an average CPU.

A retrieval example for a synthetic observation is shown in Fig. 3. The oscillating profile (red), the final SACRS solution (blue), and the FCRS solution
 310 (green), are compared with the true ozone (orange) and the a-priori (grey)

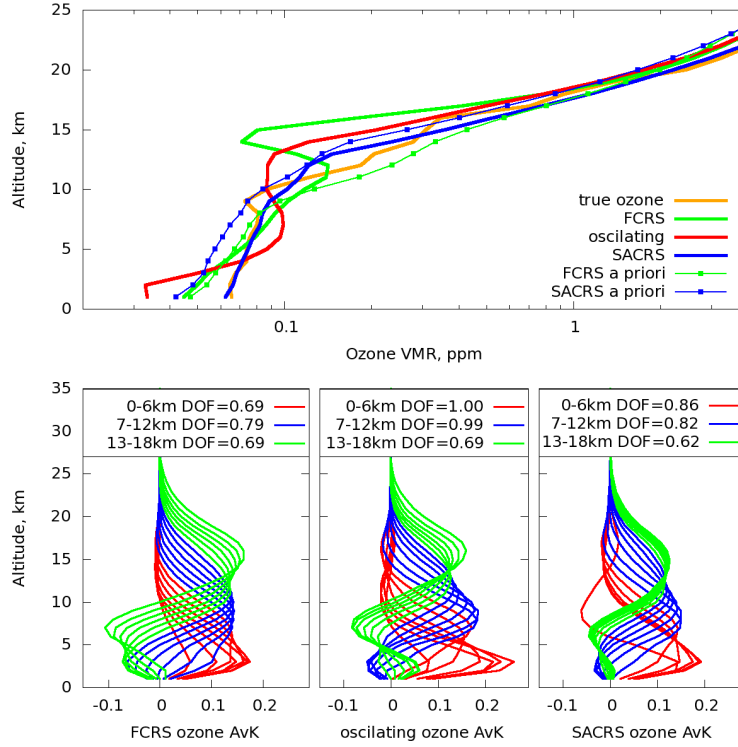


Figure 3: : The retrieval example with the corresponding AvK. The orange profile is the model used for the measurement simulation (true ozone), the green is the FCRS solution, the red profile is the oscillating solution found with the criterion of Eq. 9, the blue profile is the final result after the IVS regularization. The bottom panel shows three groups of retrieval AvK with the corresponding DOFs.

profiles without any smoothing by the AvK. In this case, the FCRS profile is close to the a priori and underestimates the true profile in the lowest 3-4 km. It overestimates the true profile above this height range and fails to reproduce the ozone gradient in the UTLS. As expected, the weakly constrained profile oscillates around the true profile. Once the a posteriori IVS regularization is applied, the SACRS profile matches well the true profile up to 9-10 km. In the UTLS, the strong oscillation introduced by the FCRS retrieval is largely reduced by the SACRS retrieval, despite remaining difficulties to retrieve small vertical features in this region due to the limited vertical resolution of the measurement.

320 The AvK in the bottom panel of Fig. 3 show that the weak constraint producing
the oscillating solution is characterized by a larger number of DOF i.e. higher
AvK values at tropospheric altitudes (red and blue AvK curves) and also in
the lower UTLS altitudes (green curves). The IVS regularization applied to the
oscillating solution provides a slightly stronger constraint: tropospheric AvK
325 become smaller than those of the oscillating solution, but still larger than those
of the FCRS solution. The corresponding DOFs are shown in the legend.

3. Simulation of the ozone pseudo-observations (PO)

The pseudo-observations or synthetic observations presented in this section
are the simulated measurements based on a known atmospheric state and the
330 corresponding forward radiative transfer calculation for the chosen instrumen-
tial configuration. In order to evaluate the performance of the SACRS algo-
rithm, two sets of pseudo-observations have been generated: one using a Chem-
istry and Transport Model (CTM) as true ozone, referred to as CTM-pseudo-
observations (CTM-PO), and one using the ozonesondes, referred to as sonde-
335 pseudo-observations(S-PO). The true ozone profiles (from CTM or sondes) are
used as the inputs of the KOPRA/KOPRAFIT radiative transfer model [37]
to simulate IASI-NG-like radiances. The radiances are simulated including the
instrumental specifications and performances of IASI-NG in terms of radiomet-
ric noise in the $10 \mu\text{m}$ spectral region ($10 \text{ nW}/(\text{cm}^2\text{srcm}^{-1})$) and the apodized
340 spectral resolution (0.25 cm^{-1}) [31]. As for the measurement geometry, we
use the IASI geometry based on the location of the pixels actually sampled
by IASI for the simulated dates. For the CTM-PO, we used the MOCAGE
(MOdèle de Chimie Atmosphérique à Grande Échelle) model [38]. This model
provides vertical profiles of atmospheric state and composition variables for 47
345 levels up to 5 hPa (approximately 35 km altitude) with a vertical resolution that
increases from 150 m (lower troposphere) to approximately 1 km (stratosphere)
and a horizontal resolution of $0.2^\circ \times 0.2^\circ$. The same set of data was used by [39]
to study multispectral ozone retrievals. We present here one day of simulations

over Europe (9 July 2010). Over 18,000 measurements have been simulated. No
350 cloud information was taken into account for these simulations.

Ozonesondes used for this study were obtained from different archives: WOUDC
(<http://www.woudc.org/>), NOAA- CMDL (<http://www.esrl.noaa.gov/gmd/dv/ftpdata.html>),
and SHADOZ (<http://croc.gsfc.nasa.gov/shadoz/>). These ozonesondes provide
in situ measurements of vertically-resolved ozone concentrations at different sta-
355 tions around the world. The measured vertical profiles of ozone have a vertical
resolution of ~ 150 m and reach up to 30–35 km. For the altitudes over 30
km, the ozone profiles in both cases (CTM-PO and S-PO) are completed with
climatological values in order to calculate the radiative transfer and the satellite
signal over the atmosphere up to 60 km of altitude corresponding to 51 layers
360 of the chosen vertical retrieval grid. For the case of S-PO only the zero de-
grees inclination nadir geometry is considered. We use, for the simulations, the
soundings available after 2007 in order to avoid using the same soundings used
to define the a priori profiles of the retrieval (section 2.1). Over 4,000 ozone
soundings have been used to simulate IASI-NG-like observations. We consider
365 the surface temperatures and the temperature profiles from ECMWF to define
the associated temperatures.

Table 1 summarizes the five retrieval sets used in the present study. The
three retrievals using the CTM-PO are performed in order to study the effect of
taking into account different sets of a priori profiles in the FCRS and compare
370 them to the SACRS retrievals using the spatially resolved ozone plumes as
the known atmospheric state. The two S-PO retrievals were made in order to
evaluate the retrievals using better vertically resolved true ozone profiles as the
known atmospheric state. The retrieval results are evaluated against the true
ozone in terms of bias, root mean square error (RMSE), and correlation. The
375 error estimate resulting from the two algorithms is evaluated using the RMSE
that represents the total error, which includes both measurement and smoothing
errors.

Table 1: Description of the simulated retrievals.

Retrieval set	Algorithm	A priori	PO-type	Simulated period	Number of obs
1	FCRS	3 a priori	CTM-PO	09.07.2010	18540
2	FCRS	11 a priori	CTM-PO	09.07.2010	18540
3	SACRS	11 a priori	CTM-PO	09.07.2010	18540
4	FCRS	3 a priori	S-PO	2007–2012	4125
5	SACRS	11 a priori	S-PO	2007–2012	4125

4. Results and discussion

First, we evaluate the impact of using the three climatological profiles or the set of eleven TPH-dependent a priori profiles (see Fig. 1) in the CTM-PO retrievals. The retrievals are made with the FCRS algorithm used in previous studies [2, 24, 4] and which includes different sets of a priori (Table 1, retrieval sets 1 and 2). Left and center panels of Fig. 4 show the results.

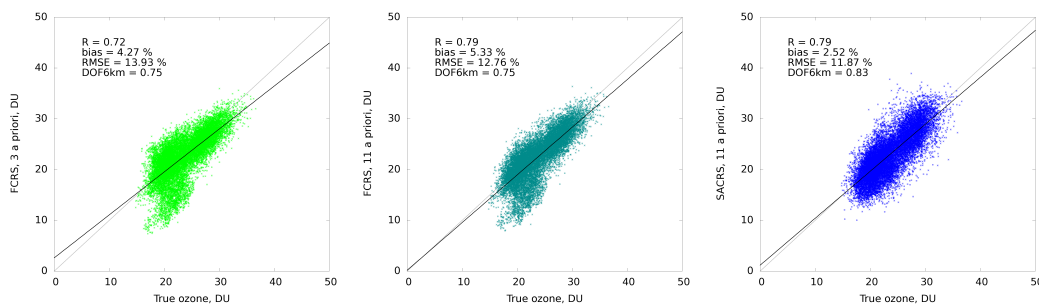


Figure 4: Scatterplots of the retrieved versus simulated ozone partial columns 0-6 km for the CTM-PO. Left panel - FCRS retrieval with the set of 3 a priori. Middle panel - FCRS retrieval with the set of 11 a priori. Right panel - SACRS retrieval with the set of 11 a priori.

The evaluation is done on the lower tropospheric ozone columns (surface-6 km) calculated in Dobson Units (DU). In order to estimate the fraction of contamination of the lower tropospheric column by higher altitudes, we calculated the ratio between the integral of the AvK of the lower tropospheric column from 6 to 60 km and the integral from the surface to 60 km. The average made for all

retrievals made for CTM-PO shows that higher atmospheric layers contribute
390 to about 20% of the lower-tropospheric column.

Using the enhanced set of a priori for FCRS improves the correlation by
about 9% of the retrievals but not the bias. The remaining tail on the scatterplot
(values < 25 DU) shows that using the enhanced a priori set does not improve
the FCRS retrieval. This tail disappears on the right panel when SACRS (Table
395 1, retrieval set 3) is used. This tail corresponds to the higher latitudes and
strong negative biases that can be seen on the map of the differences between
the retrieved and the true ozone for the case of FCRS (Fig. 5, left top panel).

The bias and the RMSE are reduced by 40% and 15% respectively when
using the SACRS approach (right panel in comparison with the left panel).
400 The correlation is also improved by about 10%. The retrieval sensitivity is also
improved using the SACRS approach with DOF 6km increased from 0.75 to
0.83 in the lower troposphere.

The true ozone distribution and the differences between the true and the
retrieved ozone distribution are shown in Fig. 5. The figure presents the results
405 obtained using the FCRS (Table 1, retrieval set 1) and SACRS (Table 1, re-
trieval set 3) approaches (first row). The spatial distribution of the DOFs for
0-6 km is also plotted for the two approaches (second row). Pixels for which at
least one of the two retrievals did not converge are displayed in white. The main
spatial features of the true ozone distribution are reproduced by both retrieval
410 schemes. Nevertheless, some overestimations and underestimations introduced
by the FCRS and already seen on the scatterplots (Fig. 4) are improved with
the SACRS, especially over the northwestern area. The lower tropospheric DOF
are increased on average using SACRS. They are more spatially homogeneous
being less dependent of the sampled atmospheric conditions (TPH, surface tem-
415 perature, thermal contrast, etc).

Two typical cases of the polar air mass retrievals are shown in Fig. 6 and
Fig. 7. The first retrieval example (Fig. 6) is taken from the Scandinavian plume
with the strong negative bias in the FCRS results shown on the maps of Fig. 5.
These polar air mass situations are characterized by low TPH (10 km) and a

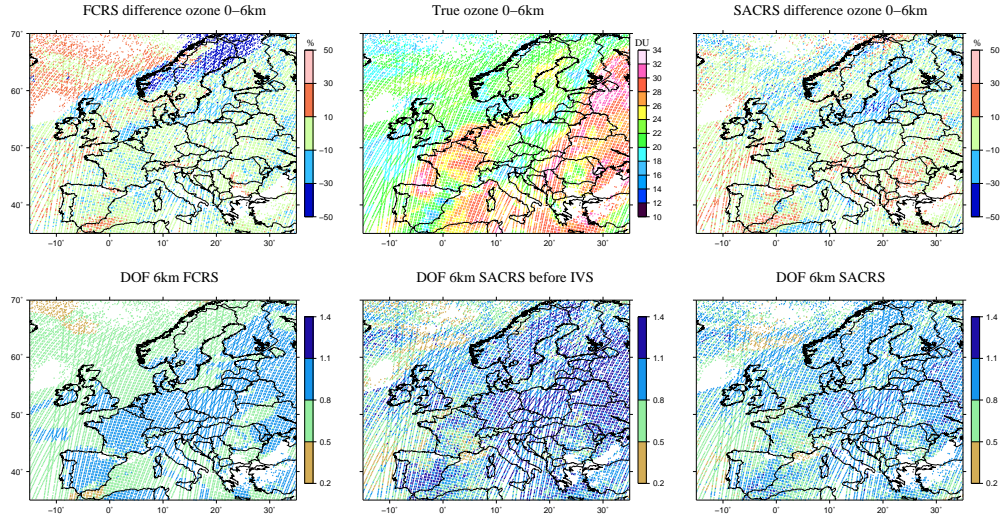


Figure 5: Distribution of the differences between the retrieved and true ozone (CTM-PO) partial columns 0-6 km (first row), retrieved DOFs for 0-6 km (second row).

420 relatively high thermal contrast (2.43 K) if compared to typical values for the polar air masses (the average thermal contrast for the simulated polar air mass cases is 0.01 K) . The second retrieval example (Fig. 7) is taken from the strong positive bias plume shown in Fig. 5 around (59.52 N, -9.24 E). These polar air mass situations are characterized by low TPH (9 km in this case) and a thermal contrast closer to zero (1.06 K in this case). The differences in the retrieved profiles can be explained by the retrieval AvK which, in the SACRS case, are better separated between the lower tropospheric part (0 km to 6 km) and the polar air mass UTLS region (7 km to 12 km). The FCRS AvK for the first polar air mass case (Fig. 6) show that almost the entire polar troposphere is correlated in this retrieval and the ozone overestimation in the lower stratosphere is compensated by the underestimation in the lower tropospheric part. In the case of the SACRS retrieval, the adapted constraint allows to better separate these two altitude regions. The AvK diagonal shows that the SACRS retrieval is less sensitive than the FCRS to the lower polar stratosphere and more sensitive

430

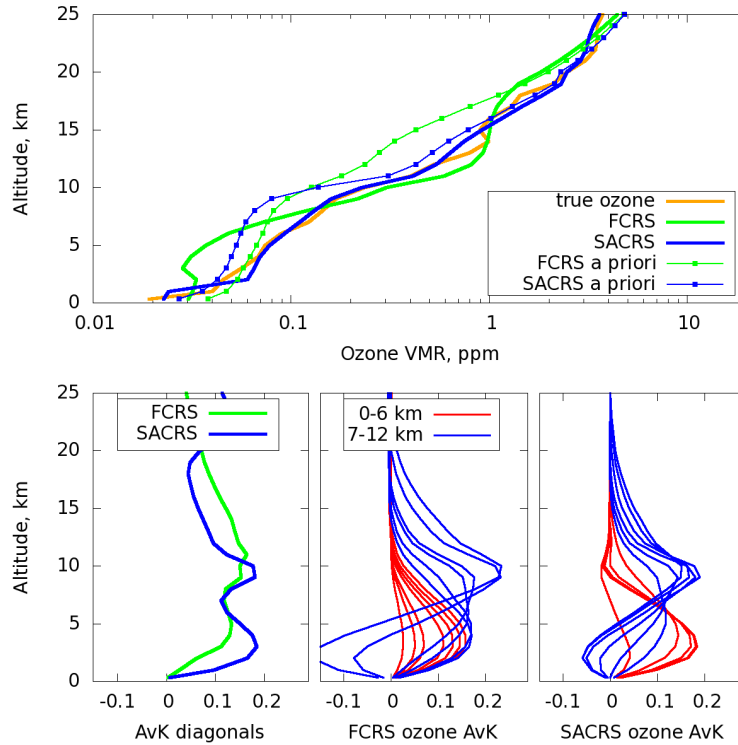


Figure 6: Example of the retrieval profiles for the polar air mass (68.56N, 21.52E).

435 to the lower tropospheric altitudes. The two maxima show the altitudes for
 which the partial columns are less inter-dependent. In the second polar air mass
 case (Fig. 7), FCRS AvK show again that almost the entire polar troposphere
 is correlated in this retrieval. This explains why the ozone underestimation
 in the lower stratosphere is compensated by the overestimation in the lower
 440 tropospheric part. The SACRS retrieval adapts the strength of the constraint
 so that the lower tropospheric part of the profile is regularized more strongly.
 The AvK diagonal shows that, as compared to the FCRS, the SACRS retrieval
 is less sensitive in the lower polar stratosphere but less correlated to the polar
 UTLS altitudes.

445 The typical case for a tropical air mass retrieval is shown in Fig. 8. This
 tropical air mass situation is characterized by high TPH (14 km). Here again the

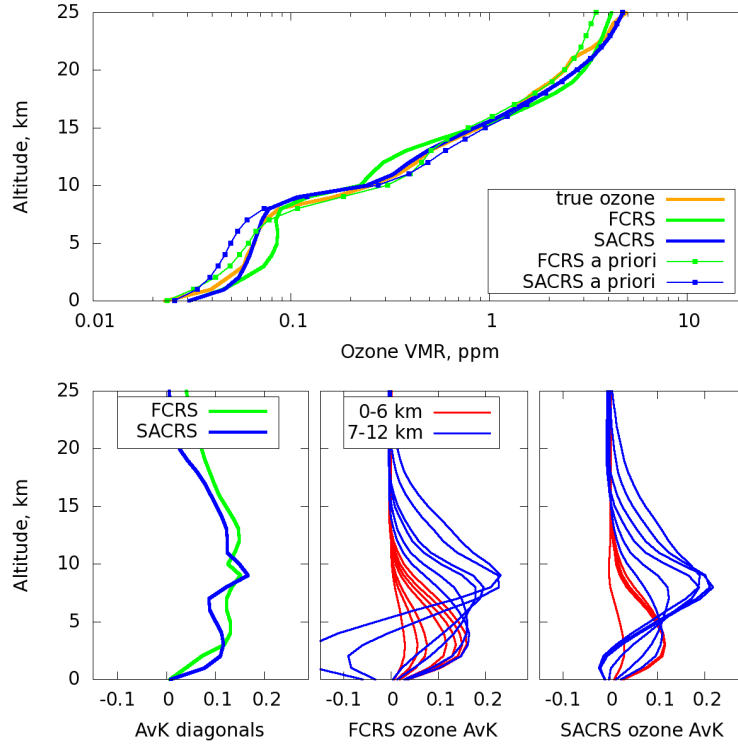


Figure 7: Example of the retrieval profiles for the polar air mass (59.52N, -9.24E).

difference between the FCRS and SACRS retrieved profiles can be explained by the differences in retrieval AvK. The self-adapting regularization of the SACRS approach constrains more effectively the profiles in the tropical UTLS region. Contrary to the FCRS retrieval, the SACRS constraint does not allow the solution vector to have the strong variations in the UTLS. In the FCRS retrieval, although the tropospheric profile is well reproduced, the ozone gradient in the UTLS region is not represented correctly.

We also evaluate the performances of the two retrieval approaches on six different partial columns in the troposphere and UTLS. We compare (Fig. 9) the correlation coefficient, the mean bias and the RMSE obtained for the different partial columns calculated between the surface and the altitude of 21 km. This evaluation is based on the CTM-PO. We see that with the SACRS approach the

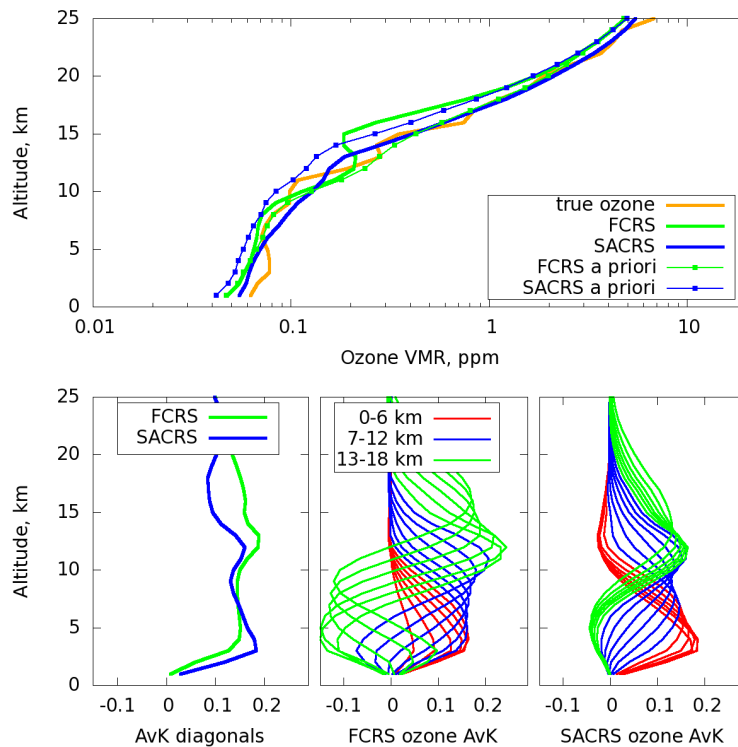


Figure 8: Example of the retrieval profiles for the tropical air mass (41.71N, 18,24E).

three statistical indicators are improved for almost all these partial columns.

460 We use the ozone soundings (Table 1, retrieval sets 4 and 5) to evaluate the retrieved profiles because they provide a sampling of a larger range of atmospheric conditions (tropical, midlatitudes and polar). In Fig. 10, the mean ozonesondes profile (averaged over the entire sounding dataset) is compared to the mean a priori profile, and the mean profiles retrieved with the FCRS and
 465 the SACRS approaches. The ozone profiles are not smoothed using the retrieval AvK for this comparison. The differences between the ozonesonde profiles and the retrieved profiles are also displayed as well as the mean diagonal of the AvK matrix which is an estimate of the sensitivity of the retrieval with respect to variations in the atmospheric true state. On average (top row), the vertical sensitivity as seen by the AvK is increased below 5 km and decreased in the UTLS
 470

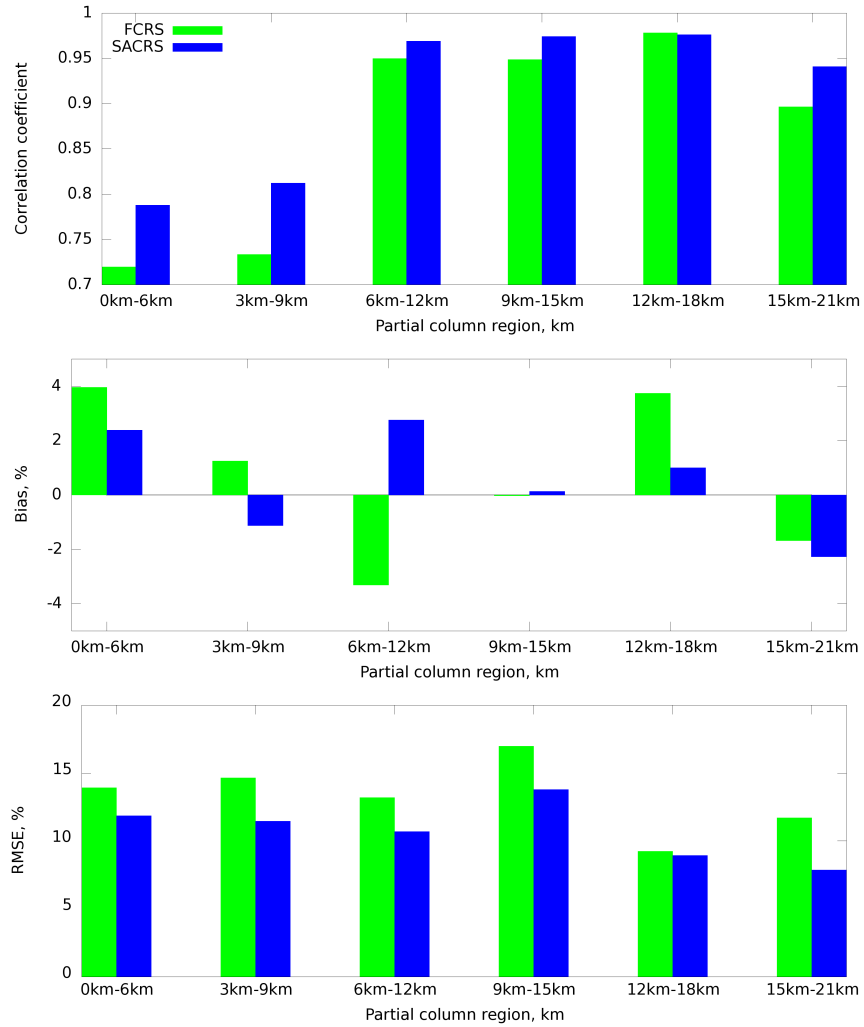


Figure 9: The 6km partial columns correlations (top), bias (middle), RMSE (bottom) for the two retrieval schemes (CTM-PO).

with the SACRS approach. The bias is more constant (about 10%) in the troposphere, up to 10 km. The bias compensation in the UTLS is strongly reduced. Considering the validation issues reported in [24, 25], we also explore the two atmospheric situations for which the FCRS approach failed more systematically: 475 the polar and the tropical latitudes (second and third rows of Fig. 10). Polar

situations are usually less favorable to the retrieval due to thermal conditions decreasing the sensitivity of infrared sounders. The SACRS approach adapts the constraint to these situations, reducing the sensitivity of the retrieval in the troposphere and then avoiding the over-interpretation of the observation. The
480 final agreement with the sondes is better with a very small bias in the troposphere. The tropospheric ozone column between 0 and 9 km calculated for these polar situations shows a bias of 8.6% with FCRS and 0.5% with SACRS. The correlation is close for both retrieval schemes: 0.87 for FCRS, 0.88 for SACRS. The underestimation of ozone in the UTLS remains. Concerning the tropics,
485 previous studies underline the difficulties to retrieve the strong ozone gradient in the UTLS region, especially due to the S-shape of the ozone profile in this region (e.g. [24]). The SACRS approach strongly improves the retrieval in the UTLS (Fig. 10 last row). The upper tropospheric ozone column between 12 and 18 km calculated for these profiles shows a bias of 24.4% with FCRS and
490 10.1% with SACRS. The correlation is also improved: 0.88 for FCRS and 0.93 for SACRS.

We also evaluate the ability of the FCRS and SACRS algorithms to prescribe realistic error estimates for both the profiles and the partial columns. We use the S-PO and the CTM-PO and compare the mean estimated error profiles,
495 which is the diagonal of the total error matrix (Eq. 5 for the FCRS and Eq. 18 for the SACRS) to the RMSE profile, which gives an estimate of the actual error. Results are provided in Fig. 11. In the case of the S-PO, the FCRS error estimation (green) is in good agreement with the actual error (RMSE) for the lower troposphere (below 7 km) and shows a strong underestimation of
500 the error at higher altitudes. The error estimation derived from the SACRS algorithm (blue) shows a slight overestimation in the lower troposphere and a good agreement for the altitudes above 8 km. Considering the CTM-PO, the SACRS error estimation is in good agreement with the actual error, whereas the FCRS error is strongly underestimated in the entire atmosphere.

505 The same behavior of the error can be seen in terms of partial columns for the case of CTM-PO: Fig. 12 presents the differences between the errors

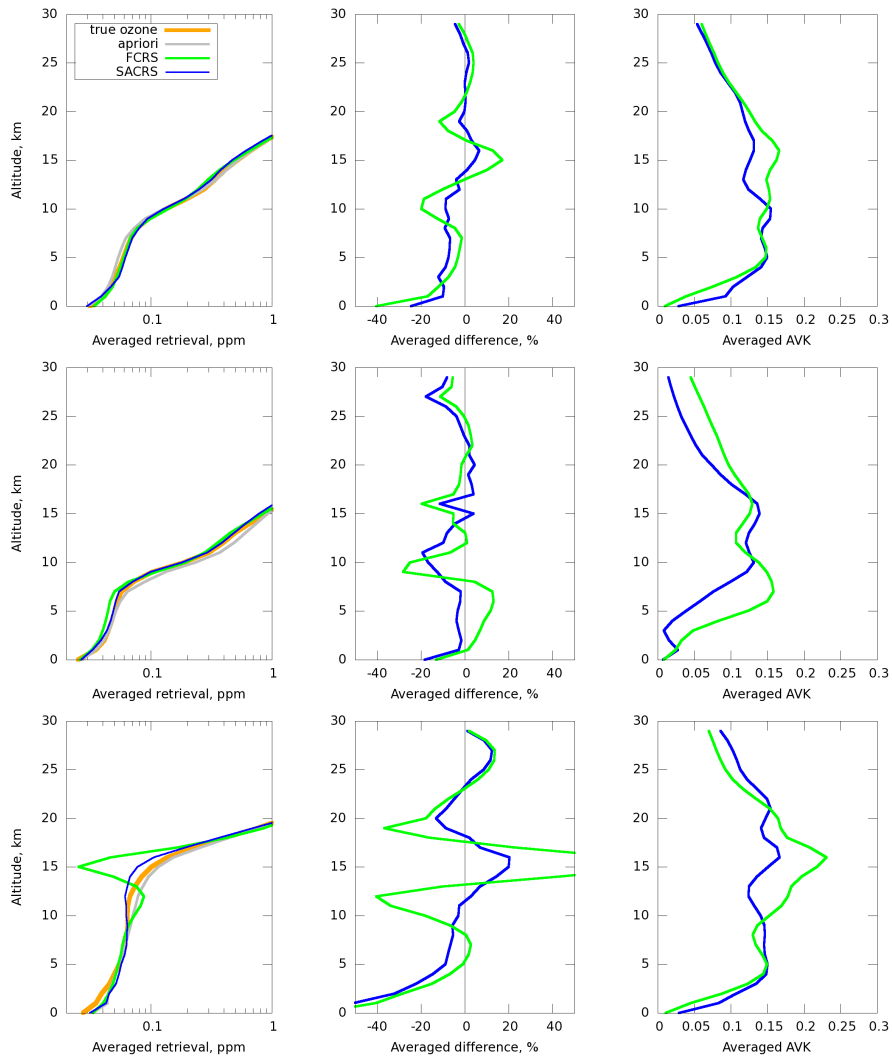


Figure 10: Simulated versus retrieved profiles from the S-PO. First row – average of the 4125 profiles (all latitudes, all stations), Second row – average of the particular cases in the polar latitudes where the DOF is decreased by self-adapting. Third row – average of the particular cases in the tropical latitudes where the retrieval of the 'S-shape' profiles is improved.

calculated as the RMSE (presented also in the Fig. 9, bottom panel) and the estimated total errors (Eq. 5 for the FCRS, and Eqs. 18 for the SACRS). These differences are shown for different retrieved partial columns between 0 and 21

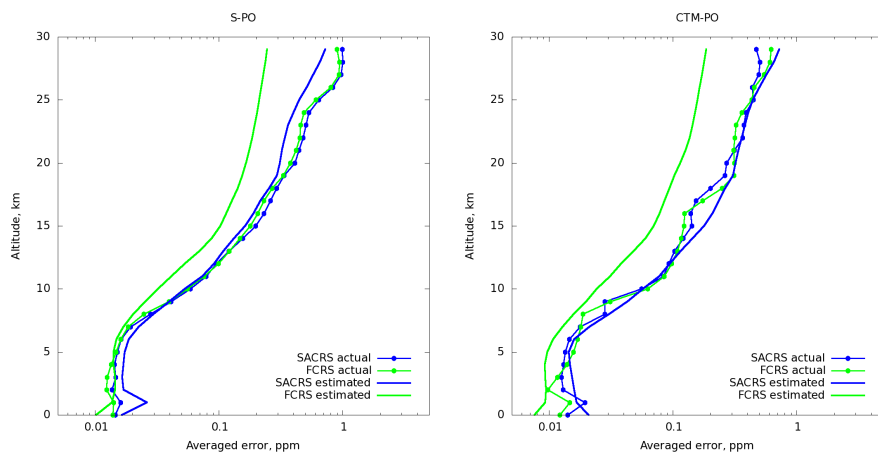


Figure 11: Estimated and actual error profiles for the S-PO retrievals (left) and for the CTM-PO retrievals (right).

510 km. The errors estimates from the FCRS approach are usually underestimated compared to the RMSE leading to a difference ranging between 6 and 14%. The SACRS reduces this difference by about 5% with a better error estimation.

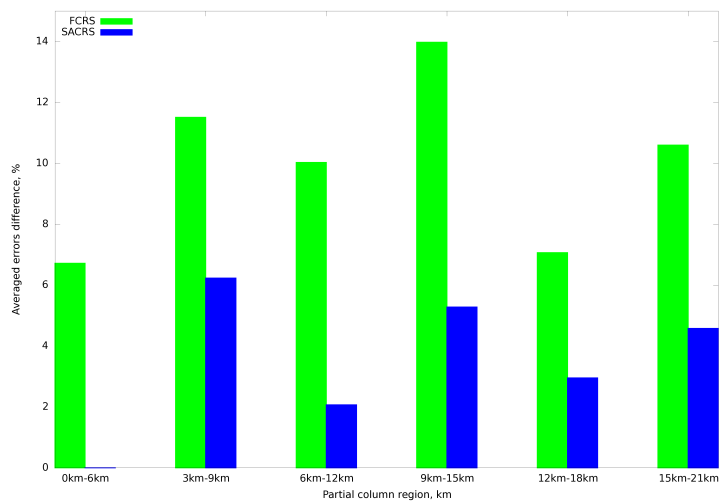


Figure 12: Differences between the estimated and the actual errors for the 6km ozone partial columns obtained by the two retrieval schemes (CTM-PO).

5. Conclusions

The SACRS has better retrieval performances in terms of bias reduction (40%), correlation improvement (10%) and RMSE reduction (15%) with respect to the FCRS. The error estimate is also in better agreement with the actual error derived from the comparison with the true ozone. The major improvements are seen for the cases of polar and tropical retrievals. Indeed, the self-adapting approach succeeds in better constraining the polar retrievals where the infrared nadir measurements usually have lower brightness temperatures and hence less information in the signal [25]. The SACRS approach performs better in the tropical cases with higher TPH where the shape of the ozone profile favors spurious oscillations in the retrieved profiles and the retrieval often may be biased in the UTLS region [24, 25]. The spatially resolved retrievals show that the lower tropospheric DOFs are increased on average using SACRS. They are more spatially homogeneous being less dependent of the sampled atmospheric conditions. The execution time for one SACRS retrieval is about 280 seconds, while for the FCRS this time is about 25 seconds. The calculation time is of course not comparable for these two retrieval schemes. The current study presents the principles of the new method to define an adjustable retrieval constraint. This retrieval scheme is not meant to be used operationally in its current state. For that purpose, an optimization of the code will be required. The new retrieval scheme was tested for instrumental specifications of the future IASI-NG instrument. Nevertheless, it may be applied to any other type of measurements. It may be particularly interesting to test this retrieval scheme with the multispectral retrievals [10, 11] where the sensitivity of the measurement to different altitudes may be highly variable due to the nature of different spectral components of the measurement and their behaviour in different atmospheric conditions. This regularization scheme may be applied to other species retrieval. The initial shape of the constraint function that is adjusted during the retrieval of the oscillating solution may be adapted to each particular species.

Acknowledgments

This study was supported by the French Space Agency CNES (project "IASI-NG-TOSCA"). Financial support of the GDRI (Groupement de Recherche
545 International) HiResMir of the CNRS is gratefully acknowledged . The HiResMir
GDRI is for "High resolution microwave, infrared and Raman molecular spectroscopy for atmospheric, planetological and astrophysical applications". We thank also Agnes Perrin (agnes.perrin@lmd.polytechnique.fr) for valuable scientific discussions during the course of this work. The ozonesonde data used
550 in this study were provided by the World Ozone and Ultraviolet Data Centre (WOUDC), the Southern Hemisphere Additional Ozonesondes (SHADOZ), and the Global Monitoring Division (GMD) of NOAA's Earth System Research Laboratory and are publicly available (see <http://www.woudc.org>, <http://croc.gsfc.nasa.gov/shadoz>,
<http://www.esrl.noaa.gov/gmd>). The authors thank all those responsible for
555 the WOUDC, SHADOZ, and GMD measurements and archives for making the ozonesonde data available.

References

- [1] F. Hilton, R. Armante, T. August, C. Barnet, A. Bouchard, C. Camy-Peyret, V. Capelle, L. Clarisse, C. Clerbaux, P.-F. Coheur, A. Collard,
560 C. Crevoisier, G. Dufour, D. Edwards, F. Fajjan, N. Fourri, A. Gambacorta, M. c. Goldberg, V. Guidard, D. Hurtmans, S. Illingworth, N. Jacquinet-Husson, T. Kerzenmacher, D. Klaes, L. Lavanant, G. Masiello, M. Matricardi, A. McNally, S. Newman, E. Pavelin, S. Payan, E. Pquignot, S. Peyridieu, T. Phulpin, J. Remedios, P. Schls sel, C. Serio, L. Strow, C. Stubenrauch, J. Taylor, D. Tobin, W. Wolf, D. Zhou, Hyperspectral earth observation from iasi: Five years of accomplishments, *Bulletin of the American Meteorological Society* 93 (3) (2012) 347-370. [arXiv:https://doi.org/10.1175/BAMS-D-11-00027.1](https://doi.org/10.1175/BAMS-D-11-00027.1), doi:10.1175/BAMS-D-11-00027.1.
565 URL <https://doi.org/10.1175/BAMS-D-11-00027.1>

- 570 [2] M. Eremenko, G. Dufour, G. Foret, C. Keim, J. Orphal, M. Beekmann, G. Bergametti, J.-M. Flaud, Tropospheric ozone distributions over Europe during the heat wave in July 2007 observed from infrared nadir spectra recorded by IASI, *Geophysical Research Letters* 35 (18). arXiv:<https://agupubs.onlinelibrary.wiley.com/doi/pdf/10.1029/2008GL034803>, doi:10.1029/2008GL034803.
575 URL <https://agupubs.onlinelibrary.wiley.com/doi/abs/10.1029/2008GL034803>
- [3] G. Dufour, M. Eremenko, J. Orphal, J.-M. Flaud, IASI observations of seasonal and day-to-day variations of tropospheric ozone over three highly
580 populated areas of China: Beijing, Shanghai, and Hong Kong, *Atmospheric Chemistry and Physics* 10 (8) (2010) 3787–3801. doi:10.5194/acp-10-3787-2010.
URL <https://www.atmos-chem-phys.net/10/3787/2010/>
- [4] G. Dufour, M. Eremenko, J. Cuesta, C. Doche, G. Foret, M. Beekmann,
585 A. Cheiney, Y. Wang, Z. Cai, Y. Liu, M. Takigawa, Y. Kanaya, J.-M. Flaud, Springtime daily variations in lower-tropospheric ozone over east Asia: the role of cyclonic activity and pollution as observed from space with IASI, *Atmospheric Chemistry and Physics* 15 (18) (2015) 10839–10856. doi:10.5194/acp-15-10839-2015.
590 URL <https://www.atmos-chem-phys.net/15/10839/2015/>
- [5] P. Kalabokas, J. Hjorth, G. Foret, G. Dufour, M. Eremenko, G. Siour, J. Cuesta, M. Beekmann, An investigation on the origin of regional springtime ozone episodes in the western Mediterranean, *Atmospheric Chemistry and Physics* 17 (6) (2017) 3905–3928. doi:10.5194/acp-17-3905-2017.
595 URL <https://www.atmos-chem-phys.net/17/3905/2017/>
- [6] C. Doche, G. Dufour, G. Foret, M. Eremenko, J. Cuesta, M. Beekmann, P. Kalabokas, Summertime tropospheric-ozone variability over the Mediterranean basin observed with IASI, *Atmospheric Chemistry and Physics*

- 14 (19) (2014) 10589–10600. doi:10.5194/acp-14-10589-2014.
600 URL <https://www.atmos-chem-phys.net/14/10589/2014/>
- [7] G. Dufour, M. Eremenko, M. Beekmann, J. Cuesta, G. Foret, A. Fortems-Cheiney, M. Lachâtre, W. Lin, Y. Liu, X. Xu, Y. Zhang, Lower tropospheric ozone over the North China Plain: variability and trends revealed by IASI satellite observations for 2008–2016, *Atmospheric Chemistry and Physics* 18 (22) (2018) 16439–16459. doi:10.5194/acp-18-16439-2018.
605 URL <https://www.atmos-chem-phys.net/18/16439/2018/>
- [8] C. Wespes, D. Hurtmans, C. Clerbaux, P.-F. Coheur, O₃ variability in the troposphere as observed by IASI over 2008–2016: Contribution of atmospheric chemistry and dynamics, *Journal of Geophysical Research: Atmospheres* 122 (4) (2017) 2429–2451. arXiv:<https://agupubs.onlinelibrary.wiley.com/doi/pdf/10.1002/2016JD025875>, doi:10.1002/2016JD025875.
610 URL <https://agupubs.onlinelibrary.wiley.com/doi/abs/10.1002/2016JD025875>
- [9] S. Safieddine, A. Boynard, P.-F. Coheur, D. Hurtmans, G. Pfister, B. Quennehen, J. L. Thomas, J.-C. Raut, K. S. Law, Z. Klimont, J. Hadji-Lazaro, M. George, C. Clerbaux, Summertime tropospheric ozone assessment over the Mediterranean region using the thermal infrared IASI/MetOp sounder and the WRF-Chem model, *Atmospheric Chemistry and Physics* 14 (18) (2014) 10119–10131. doi:10.5194/acp-14-10119-2014.
620 URL <https://www.atmos-chem-phys.net/14/10119/2014/>
- [10] J. Cuesta, M. Eremenko, X. Liu, G. Dufour, Z. Cai, M. Höpfner, T. von Clarmann, P. Sellitto, G. Foret, B. Gaubert, M. Beekmann, J. Orphal, K. Chance, R. Spurr, J.-M. Flaud, Satellite observation of lowermost tropospheric ozone by multispectral synergism of IASI thermal infrared and GOME-2 ultraviolet measurements over Europe, *Atmospheric Chemistry*
625

and Physics 13 (19) (2013) 9675–9693. doi:10.5194/acp-13-9675-2013.
URL <https://www.atmos-chem-phys.net/13/9675/2013/>

[11] J. Cuesta, Y. Kanaya, M. Takigawa, G. Dufour, M. Eremenko, G. Foret,
630 K. Miyazaki, M. Beekmann, Transboundary ozone pollution across
East Asia: daily evolution and photochemical production analysed by
IASI + GOME2 multispectral satellite observations and models, Atmospheric
Chemistry and Physics 18 (13) (2018) 9499–9525. doi:10.5194/
acp-18-9499-2018.

635 URL <https://www.atmos-chem-phys.net/18/9499/2018/>

[12] C. D. Rodgers, Inverse methods for atmospheric sounding : theory and
practice, World Scientific Publishing, 2000.

[13] A. Boynard, C. Clerbaux, P.-F. Coheur, D. Hurtmans, S. Turquety,
M. George, J. Hadji-Lazaro, C. Keim, , J. Meyer-Arnek, Measurements
640 of total and tropospheric ozone from IASI: comparison with correlative
satellite, ground-based and ozonesonde observations, Atmospheric Chem-
istry and Physics 9 (2009) 6255–6271. doi:10.5194/acp-9-6255-2009.

URL <https://www.atmos-chem-phys.net/9/6255/2009/>

[14] B. Barret, E. Le Flochmoen, B. Sauvage, E. Pavelin, M. Matricardi, J. P.
645 Cammas, The detection of post-monsoon tropospheric ozone variability
over south Asia using IASI data, Atmospheric Chemistry and Physics 11
(2011) 9533–9548. doi:10.5194/acp-11-9533-2011.

URL [https://www.atmos-chem-phys.net/11/9533/2011/
acp-11-9533-2011.html](https://www.atmos-chem-phys.net/11/9533/2011/acp-11-9533-2011.html)

650 [15] A. Carissimo, I. De Feis, C. Serio, The Physical Retrieval Methodology for
IASI: The delta-IASI Code, Environmental Modelling and Software 20 (9)
(2005) 1111–1126. doi:10.1016/j.envsoft.2004.07.003.

URL <http://dx.doi.org/10.1016/j.envsoft.2004.07.003>

[16] G. Liuzzi, G. Masiello, C. Serio, S. Venafrà, C. Camy-Peyret, Physical
655 inversion of the full IASI spectra: Assessment of atmospheric parameters

retrievals, consistency of spectroscopy and forward modelling, *Journal of Quantitative Spectroscopy and Radiative Transfer* 182 (2016) 128–157. doi:<https://doi.org/10.1016/j.jqsrt.2016.05.022>.

URL <http://www.sciencedirect.com/science/article/pii/S0022407316301248>

660

[17] A. Tikhonov, On the regularization of ill-posed problems, *Dokl. Acad. Nauk SSSR* 153 (1963) 49–52.

[18] S. Twomey, On the numerical solution of Fredholm integral equations of the first kind by the inversion of the linear system produced by quadrature, *J. Ass. Comput. Mach.* 10 (1963) 97–101. doi:doi:10.1145/321150.321157.

665

[19] B. C. Phillips, A technique for the numerical solution of certain integral equations of the first kind, *J. Ass. Comput. Mach.* 9 (1962) 84–97. doi:doi:10.1145/321105.321114.

[20] S. S. Kulawik, G. Osterman, D. B. A. Jones, K. W. Bowman, Calculation of altitude-dependent tikhonov constraints for TES nadir retrievals, *IEEE Transactions on Geoscience and Remote Sensing* 44 (5) (2006) 1334–1342. doi:10.1109/TGRS.2006.871206.

670

[21] K. Levenberg, A Method for the Solution of Certain Problems in Least Squares, *Quart. Appl. Math.* 2 (1944) 164–168.

[22] D. Marquardt, An Algorithm for Least-Squares Estimation of Nonlinear Parameters, *SIAM J. Appl. Math.* 11 (1963) 431–441.

675

[23] C. Keim, M. Eremenko, J. Orphal, G. Dufour, J.-M. Flaud, M. Höpfner, A. Boynard, C. Clerbaux, S. Payan, P.-F. Coheur, D. Hurtmans, H. Claude, H. Dier, B. Johnson, H. Kelder, R. Kivi, T. Koide, M. López Bartolomé, K. Lambkin, D. Moore, F. J. Schmidlin, R. Stübi, Tropospheric ozone from IASI: comparison of different inversion algorithms and validation with ozone sondes in the northern middle latitudes, *Atmospheric Chemistry and*

680

Physics 9 (24) (2009) 9329–9347. doi:10.5194/acp-9-9329-2009.

URL <https://hal.archives-ouvertes.fr/hal-00382538>

- 685 [24] G. Dufour, M. Eremenko, A. Griesfeller, B. Barret, E. LeFlochmoën,
C. Clerbaux, J. Hadji-Lazaro, P.-F. Coheur, D. Hurtmans, Validation of
three different scientific ozone products retrieved from IASI spectra using
ozonesondes, Atmospheric Measurement Techniques 5 (3) (2012) 611–630.
doi:10.5194/amt-5-611-2012.

690 URL <https://www.atmos-meas-tech.net/5/611/2012/>

- [25] A. Boynard, D. Hurtmans, M. E. Koukouli, F. Goutail, J. Bureau, S. Safied-
dine, C. Lerot, J. Hadji-Lazaro, C. Wespes, J.-P. Pommereau, A. Pazmino,
I. Zyrichidou, D. Balis, A. Barbe, S. N. Mikhailenko, D. Loyola, P. Valks,
M. Van Roozendaal, P.-F. Coheur, C. Clerbaux, Seven years of IASI ozone
695 retrievals from FORLI: validation with independent total column and ver-
tical profile measurements, Atmospheric Measurement Techniques 9 (9)
(2016) 4327–4353. doi:10.5194/amt-9-4327-2016.

URL <https://www.atmos-meas-tech.net/9/4327/2016/>

- [26] R. Nassar, J. A. Logan, H. M. Worden, I. A. Megretskaia, K. W. Bow-
700 man, G. B. Osterman, A. M. Thompson, D. W. Tarasick, S. Austin,
H. Claude, M. K. Dubey, W. K. Hocking, B. J. Johnson, E. Joseph,
J. Merrill, G. A. Morris, M. Newchurch, S. J. Oltmans, F. Posny,
F. J. Schmidlin, H. Vmel, D. N. Whiteman, J. C. Witte, Validation
of Tropospheric Emission Spectrometer (TES) nadir ozone profiles us-
ing ozonesonde measurements, Journal of Geophysical Research: Atmo-
spheres 113 (D15). arXiv:[https://agupubs.onlinelibrary.wiley.com/
doi/pdf/10.1029/2007JD008819](https://agupubs.onlinelibrary.wiley.com/doi/pdf/10.1029/2007JD008819), doi:10.1029/2007JD008819.

705 URL [https://agupubs.onlinelibrary.wiley.com/doi/abs/10.1029/
2007JD008819](https://agupubs.onlinelibrary.wiley.com/doi/abs/10.1029/2007JD008819)

- 710 [27] H. M. Worden, J. A. Logan, J. R. Worden, R. Beer, K. Bowman,
S. A. Clough, A. Eldering, B. M. Fisher, M. R. Gunson, R. L.

- Herman, S. S. Kulawik, M. C. Lampel, M. Luo, I. A. Megretskaia, G. B. Osterman, M. W. Shephard, Comparisons of Tropospheric Emission Spectrometer (TES) ozone profiles to ozonesondes: Methods and initial results, *Journal of Geophysical Research: Atmospheres* 112 (D3). arXiv:<https://agupubs.onlinelibrary.wiley.com/doi/pdf/10.1029/2006JD007258>, doi:10.1029/2006JD007258.
URL <https://agupubs.onlinelibrary.wiley.com/doi/abs/10.1029/2006JD007258>
- 715
- [28] S. S. Kulawik, K. W. Bowman, M. Luo, C. D. Rodgers, L. Jourdain, Impact of nonlinearity on changing the a priori of trace gas profile estimates from the Tropospheric Emission Spectrometer (TES), *Atmospheric Chemistry and Physics* 8 (12) (2008) 3081–3092. doi:10.5194/acp-8-3081-2008.
URL <https://www.atmos-chem-phys.net/8/3081/2008/>
- 720
- [29] J. C. Wei, L. L. Pan, E. Maddy, J. V. Pittman, M. Divarkarla, X. Xiong, C. Barnet, Ozone Profile Retrieval from an Advanced Infrared Sounder: Experiments with Tropopause-Based Climatology and Optimal Estimation Approach, *Journal of Atmospheric and Oceanic Technology* 27 (7) (2010) 1123–1139. arXiv:<https://doi.org/10.1175/2010JTECHA1384.1>, doi:10.1175/2010JTECHA1384.1.
URL <https://doi.org/10.1175/2010JTECHA1384.1>
- 725
- [30] J. Bak, X. Liu, J. C. Wei, L. L. Pan, K. Chance, J. H. Kim, Improvement of OMI ozone profile retrievals in the upper troposphere and lower stratosphere by the use of a tropopause-based ozone profile climatology, *Atmospheric Measurement Techniques* 6 (9) (2013) 2239–2254. doi:10.5194/amt-6-2239-2013.
URL <https://www.atmos-meas-tech.net/6/2239/2013/>
- 730
- [31] C. Crevoisier, C. Clerbaux, V. Guidard, T. Phulpin, R. Armante, B. Barret, C. Camy-Peyret, J.-P. Chaboureau, P.-F. Coheur, L. Crépeau, G. Dufour, L. Labonnote, L. Lavanant, J. Hadji-Lazaro, H. Herbin, N. Jacquinet-
- 740

- Husson, S. Payan, E. Péquignot, C. Pierangelo, P. Sellitto, C. Stubenrauch, Towards IASI-New Generation (IASI-NG): impact of improved spectral resolution and radiometric noise on the retrieval of thermodynamic, chemistry and climate variables, *Atmospheric Measurement Techniques* 7 (12) (2014) 4367–4385. doi:10.5194/amt-7-4367-2014.
URL <https://www.atmos-meas-tech.net/7/4367/2014/>
- [32] P. Sellitto, G. Dufour, M. Eremenko, J. Cuesta, P. Dauphin, G. Forêt, B. Gaubert, M. Beekmann, V.-H. Peuch, J.-M. Flaud, Analysis of the potential of one possible instrumental configuration of the next generation of IASI instruments to monitor lower tropospheric ozone, *Atmospheric Measurement Techniques* 6 (3) (2013) 621–635. doi:10.5194/amt-6-621-2013.
URL <https://www.atmos-meas-tech.net/6/621/2013/>
- [33] M. Ridolfi, L. Sgheri, A self-adapting and altitude-dependent regularization method for atmospheric profile retrievals, *Atmospheric Chemistry and Physics* 9 (6) (2009) 1883–1897. doi:10.5194/acp-9-1883-2009.
URL <https://www.atmos-chem-phys.net/9/1883/2009/>
- [34] M. Ridolfi, L. Sgheri, Iterative approach to self-adapting and altitude-dependent regularization for atmospheric profile retrievals, *Opt. Express* 19 (27) (2011) 26696–26709. doi:10.1364/OE.19.026696.
URL <http://www.opticsexpress.org/abstract.cfm?URI=oe-19-27-26696>
- [35] P. Raspollini, B. Carli, M. Carlotti, S. Ceccherini, A. Dehn, B. M. Dinelli, A. Dudhia, J.-M. Flaud, M. López-Puertas, F. Niro, J. J. Remedios, M. Ridolfi, H. Sembhi, L. Sgheri, T. von Clarmann, Ten years of MIPAS measurements with ESA Level 2 processor V6 Part 1: Retrieval algorithm and diagnostics of the products, *Atmospheric Measurement Techniques* 6 (9) (2013) 2419–2439. doi:10.5194/amt-6-2419-2013.
URL <https://www.atmos-meas-tech.net/6/2419/2013/>

- 770 [36] T. Steck, Methods for determining regularization for atmospheric retrieval problems, *Appl. Opt.* 41 (9) (2002) 1788–1797. doi:10.1364/AO.41.001788.
URL <http://ao.osa.org/abstract.cfm?URI=ao-41-9-1788>
- [37] G. P. Stiller, M. Hoepfner, M. Kuntz, T. von Clarmann, G. Echle, H. Fischer, B. Funke, N. Glatthor, F. Hase, H. Kemnitzer, S. Zorn, Karlsruhe
775 optimized and precise radiative transfer algorithm: I. Requirements, justification, and model error estimation (1998). doi:10.1117/12.317754.
URL <https://doi.org/10.1117/12.317754>
- [38] B. Josse, P. Simon, V.-H. Peuch, Radon global simulations with the multiscale chemistry and transport model MOCAGE, *Tellus B* 56 (4) (2004)
780 339–356. arXiv:<https://onlinelibrary.wiley.com/doi/pdf/10.1111/j.1600-0889.2004.00112.x>, doi:10.1111/j.1600-0889.2004.00112.x.
URL <https://onlinelibrary.wiley.com/doi/abs/10.1111/j.1600-0889.2004.00112.x>
- [39] L. Costantino, J. Cuesta, E. Emili, A. Coman, G. Foret, G. Dufour, M. Eremenko, Y. Chailleux, M. Beekmann, J.-M. Flaud, Potential of multispectral synergism for observing ozone pollution by combining IASI-NG and UVNS measurements from the EPS-SG satellite, *Atmospheric Measurement Techniques* 10 (4) (2017) 1281–1298. doi:10.5194/amt-10-1281-2017.
785
790 URL <https://www.atmos-meas-tech.net/10/1281/2017/>